Observations of hail cores of tornadic thunderstorms with three polarimetric radars

Valery Melnikov, Dusan Zrnic, Donald Burgess, and Edward Mansell

The University of Oklahoma, CIMMS and National Severe Storms Laboratory, Norman, OK.

1. Introduction

Supercell thunderstorms typically produce hail. The largest hail is commonly found at the edges of the updrafts, which allow sufficient growth time for hail to reach large sizes (Miller et al. 1988). An algorithm for hail recognition with the single polarization WSR-88D (Weather Surveillance Radar-Doppler) has been in use since early 1990s (Witt et al. 1994). Dual polarization radar capabilities allow measurements of differential reflectivity (Z_{DR}, dB), correlation coefficient (ρ_{hv}), and differential phase (Φ_{dp}), which deliver additional information about scatterers. Studies by Balakrishnan and Zrnic (1990) of hail producing thunderstorms reveal low Z_{DR} (about 0 dB) and reduced ρ_{hv} (down to 0.8) in hail cores. These features are explained with tumbling non-spherical hailstones: the correlation coefficient drops because the scatterers are not spherical and Z_{DR} is low because they tumble. Further works reveal variety of hail cases with reflectivities in a wide interval from ~ 30 to over 60 dBZ, with ZDR in the interval from -1 to 3 dB and ρ_{hv} in the interval from 0.4 to 0.9 (e.g., Ryzhkov et al. 2005b; Heinselman and Ryzhkov 2006, Picca and Ryzhkov2012).

Hail producing thunderstorms exhibit variety of polarimetric properties in their cores. Such variations are explained with variations in the hailstone shape and sizes, their kinematic characteristics (tumbling and precession/rotation), presence of water on hailstones' surfaces, and resonant scattering effects. The polarimetric characteristics of hail cores are typically explored for a given wavelengths. In this study we analyze data collected with different radars in the same areas of storms (section 2) and study dependencies of polarimetric properties upon radar characteristics such as operating frequencies and the system differential phase (section 3). We also discuss some new polarimetric features observed in hailstorms (section 4).

2. Radar data

2.1. Radar systems

Tornadic hailstorms developed in central Oklahoma in May 2013 were observed with four polarimetric radars: three WSR-88Ds and a mobile X band system. These are WSR-88D KOUN and KCRI located in Norman, OK within a short distance of 230 m from each other. The third WSR-88D was KTLX system located at azimuth of 57^{o} and 19.95 km away from KOUN/KCRI. The WSR-88Ds operate at S frequency band. NOXP radar is a 3-cm wavelength system; it was deployed about 65 m from the KOUN's tower for the experiment (Fig. 1). To reduce the levels of interference signals, the WSR-88Ds operate at different frequencies which are listed in Table 1.

Fig. 1. NOXP deployed next to the KOUN's tower.

Table 1. Operating frequencies of the WSR-88Ds and NOXP.

Radar	Frequency, MHz	Frequency band
KOUN	2705	S
KTLX	2910	S
KCRI	2995	S
NOXP	9410	X

The WSR-88Ds and NOXP employ a polarization configuration with Simultaneous Transmission And Reception (STAR) of horizontally and vertically polarized waves. The NOXP antenna is a scaled down version of the WSR-88D's antenna. Both antennas have equal beamwidths of 0.95^o. Due to strong attenuation of 3-cm wavelength radiation in thunderstorm, NOXP is not a good system for observations of hail thunderstorms which is demonstrated in the next section. So the data have been analyzes from the three WSR-88s operating at different frequencies. Our main goal of this communication is an analysis of impacts of different radar frequencies and phase characteristics on observed reflectivity, Z_{DR} and ρ_{hv}.

Attenuation in hail producing thunderstorms is significant and has to be corrected. Corrections for reflectivity (ΔZ) and differential reflectivity (ΔZ_{DR}) in data obtained with the WSR-88Ds is made by using measured differential phase Φ_{DP} as follows (e.g., Bringi et al., 1990),

$$\Delta Z = 0.04\ \Phi_{DP}, \quad \Delta Z_{DR} = 0.004\ \Phi_{DP},$$

where ΔZ and ΔZ_{DR} are in dB and Φ_{DP} is in degrees. Values of ΔZ and ΔZ_{DR} are added to measured Z and Z_{DR} because we used the Level II radar data, which are not corrected for attenuation.

2.2. Event 31 May 2013

Radar images of tornado and hail producing thunderstorm observed 31 May, 2013 with the four radars are shown in Fig. 2. The images at lowest antenna elevation of 0.5^o are presented. The storm produced EF3 tornado at the time; the tornado was located in the hook echo area. The tornadic area is surrounded with an arc of high reflectivity to the North from the tornado vortex; this arc indicated with "1" in the figure. The area with tornado mesocyclone has low Z_{DR} and the tornado debris ball has low ρ_{hv} (Fig 2). The Z_{DR} arc is seen along the inflow edge of the storm. These features are typical for tornadic storms (Kumjian and Ryzhkov 2008, 2009, Schwarz and Burgess 2011) and can be seen in images from the three radars.

One can see that X-band radiation experienced severe attenuation: only front areas of the thunderstorm were observed with NOXP. Luckily, the tornado occurred at a cloud fringe close to the radar so it was observed by NOXP. Severe attenuation made Z_{DR} from NOXP negative at the far fringes of observed echoes. Due to tremendous attenuation NOXP's data cannot be used for analyzing hail cores in this event.

An area of strong reflectivity to the North from the tornado mesocyclone did not have reports of hail on the ground. Large hail with sizes up to 6 cm was produced by the ridge of high reflectivity indicated with number '2' in Fig. 2 (see the top left panel). Maximal reflectivity values from these two areas were about 63-67 dBZ, i.e., about the same. To compare radar polarimetric characteristics from the areas, values of Z_{DR} and ρ_{hv} have been presented as function of reflectivity for the reflectivity values larger than 40 dBZ. This threshold have been chosen since probability of hail increases sharply for reflectivity values exceeding 50 dB (Witt et al. 1994) but it is known that hail can be produced in areas with reflectivities as low as 30 dB.

Figs. 3(a,b) present the mean Z_{DR} and ρ_{hv} as a function of reflectivity for area '1'. Similar graphs for area '2' are shown in Figs. 3(c,d). The mean values are indicated with brackets, i.e., $<Z_{DR}>$ and $<\rho_{hv}>$. In Figs. 3(a,b) one can see that $<Z_{DR}>$ increase with Z. This feature is opposite to usual expectations that Z_{DR} and ρ_{hv} should decrease with Z in hail areas. It is also seen that $<Z_{DR}>$ from KOUN exceed the values from KTLX by 1 dB, which is significant and cannot be explained with miscalibrations of differential reflectivity in the systems. The values of ZDR are high and reach 3-4 dB for very large Z. This dependence is likely caused by small melting hail having toroidal water layers. Values of $<\rho_{hv}>$ as function of Z from the three radars do not exhibit similar behaviors (Fig. 3b): the correlation coefficient (CC) from KOUN and KCRI increase with Z whereas CC from KTLX drops at Z > 57 dB.

In area '2'(the hail core), one can see that Z_{DR} increase with Z for KOUN and remains rather constant for KCRI and KTLX (Fig. 3c). All radars exhibit rather high Z_{DR} values. The values of ρ_{hv} are in the interval from 0.94 to 0.98 (Fig. 3d); The mean CC from KOUN increase with Z whereas other two radars show a decrease.

One more feature should be noticed in Fig. 3: the maximal reflectivity value from KOUN is noticeably larger than the values from the other radars. In Figs. 3ab, this difference reaches 7-8 dB.

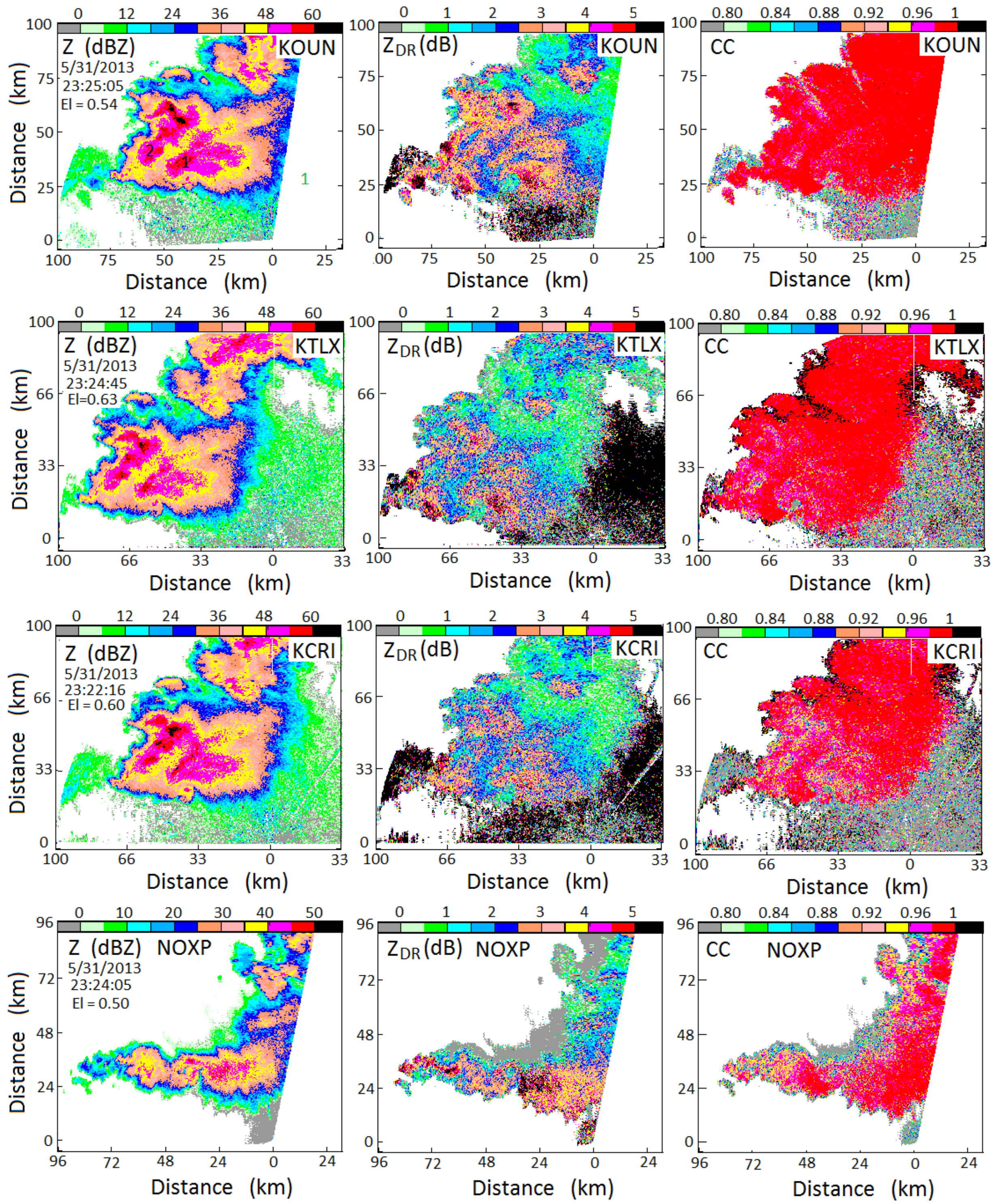

Fig. 2. Polarimetric fields of tornadic thunderstorm on May 31, 2013 at about 23:24 UTC. The data were collected with KOUN, KTLX, KCRI, and NOXP at the time of strong EF3 tornado near El Reno, OK.

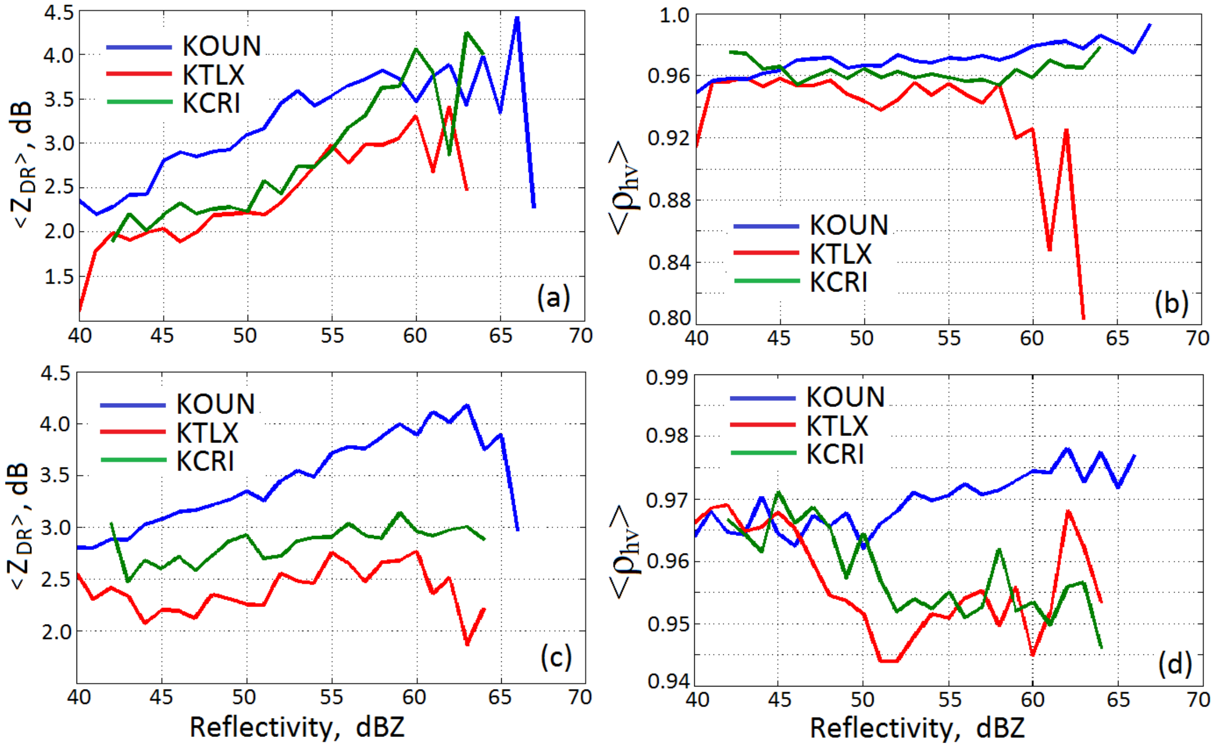

Fig. 3. (a): The mean Z_{DR} as a function of reflectivity for an area of high reflectivity indicated with "1" in the left top panel of Fig. 2. (b): Same as in (a) but for the mean correlation coefficients. (c,d): Same as in (a,b) but for high reflectivity core designated with "2" in the left top panel of Fig. 2.

Fig. 4 presents polarimetric fields from the four radars at about 00:24 UTC on June 1, 2013 when a giant hail was observed on the ground in area '2'. An example of a hailstone is shown in Fig. 5 and its location is shown in the left top panel of Fig. 4 with a circle (to the north-west from '1'). The largest reported hailstone sizes were about 7 cm (2.7 inch). X band radiation experienced severe attenuation as in the previous case therefore the southern thunderstorm's fringe was only visible for NOXP radar.

Fig 6 presents the mean $<Z_{DR}>$ and $<\rho_{hv}>$ as functions of reflectivity as in Fig. 3. Maximal reflectivities in area '2' (left bottom panels in Fig. 6) were about the same whereas in area '1'(Figs. 6 ab), maximal reflectivity from KOUN is 5 dB higher than that from KCRI and KTLX. One can see that in area '1", $<Z_{DR}>$ increase with Z and reach 3-4 dB at maximal Z. This is similar to Fig. 3a. The difference between $<Z_{DR}>$ from KOUN and KTLX is about 1 dB. The values of $<\rho_{hv}>$ from KOUN show some increase with Z whereas the values from other radars remain rather the same (Fig. 6b).

In area '2' (giant hail), there is no definite dependence $<Z_{DR}>$ upon Z: $<Z_{DR}>$ remain about the same for each radar but difference between curves for KOUN and KTLX remains about 1 dB for Z > 50 dB (Fig. 6c). The values of $<\rho_{hv}>$ from KOUN do not show big difference in areas '1' and '2' whereas for the other two radars, $<\rho_{hv}>$ drop from 0.96-0.97 to 0.94-0.96 at Z > 50 dB (Fig. 6d).

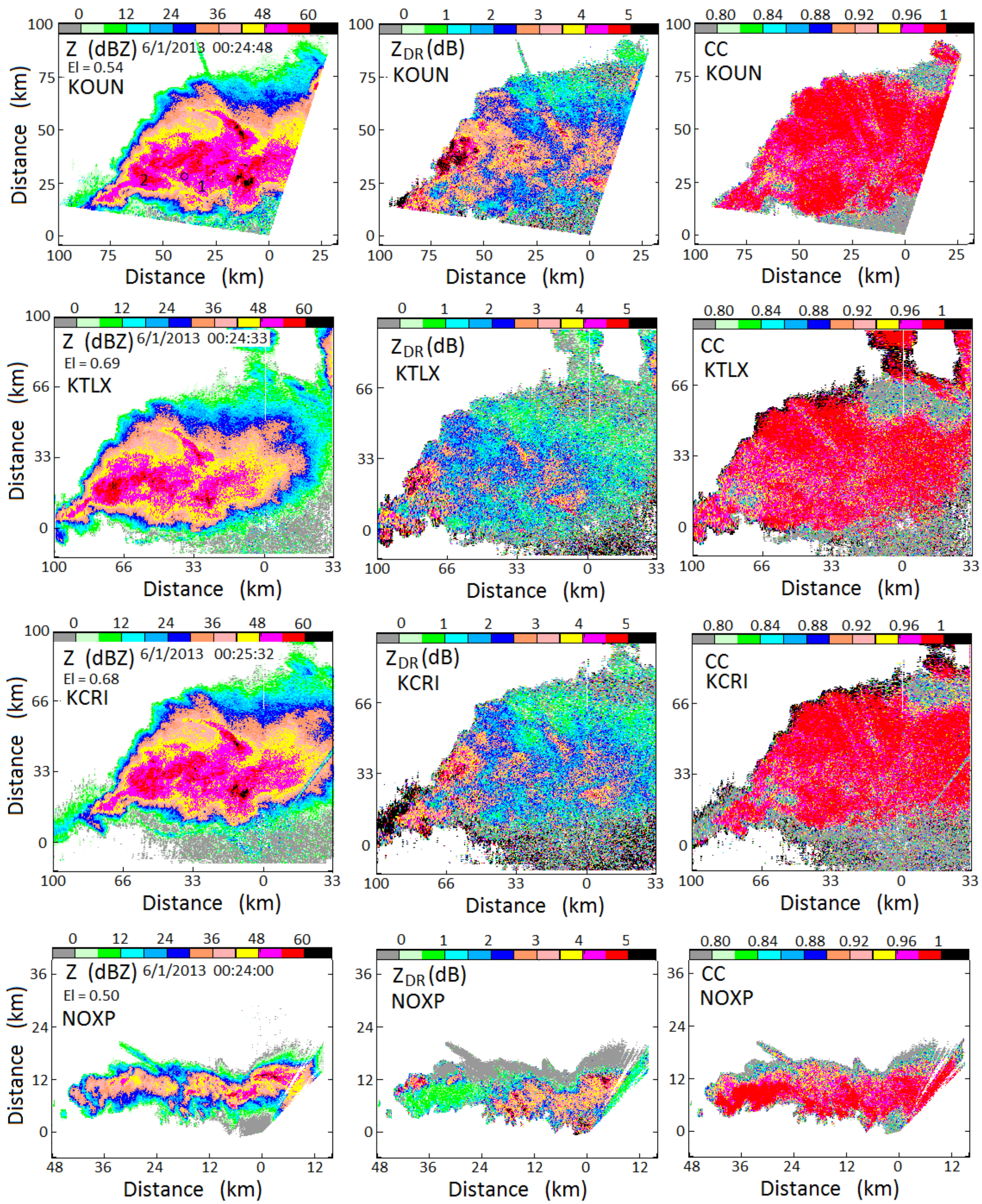

Fig. 4. Polarimetric fields collected with KOUN, KTLX, KCRI, and NOXP on June 6, 2013 at 0024 about the time of observed giant hail on the ground. The location of giant hail is show with a circle in the left top panel (to the north-west from '1').

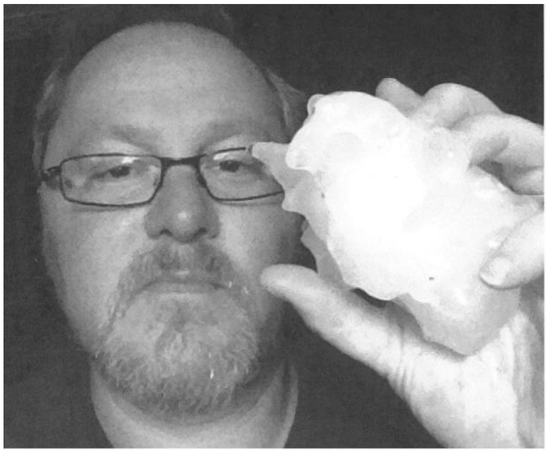

Fig. 5. A giant hailstone picked up by Mr. Coleman Harrison in city of El Reno, OK 6/1/2013 at about 0025 Z. Courtesy of C. Harrison and R. Doviak.

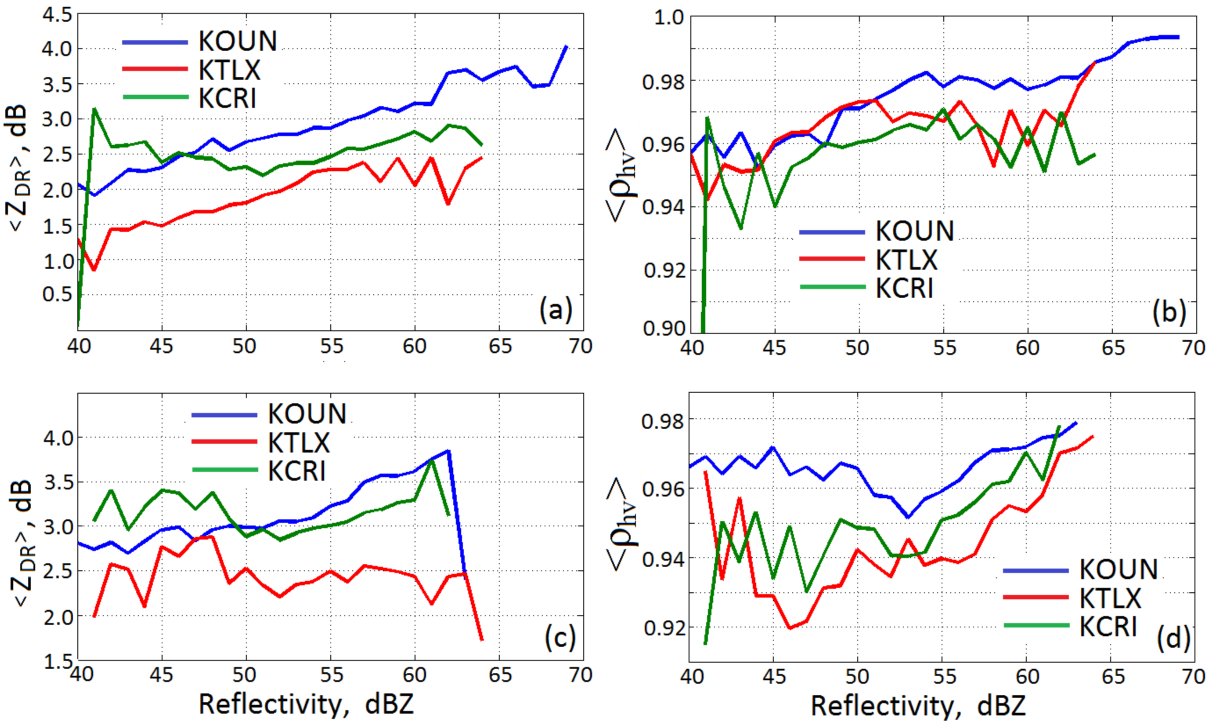

Fig. 6. (a): The mean Z_{DR} as a function of reflectivity for an area of enhanced reflectivity in area "1'. (b): Same as in (a) but for the mean correlation coefficients. (c,d): Same as in (a,b) but for high reflectivity core designated with "2" in the left top panel of Fig. 4.

2.3. *Event 19 May 2013*

Fig. 7 presents polarimetric fields collected 19 May, 2013 in the tornadic thunderstorm that struck east of Norman, OK. The tornado was spawned in the hook echo in the southern fringe of radar echo. Hail with sizes of 4 cm was observed in the area of strongest reflectivity.

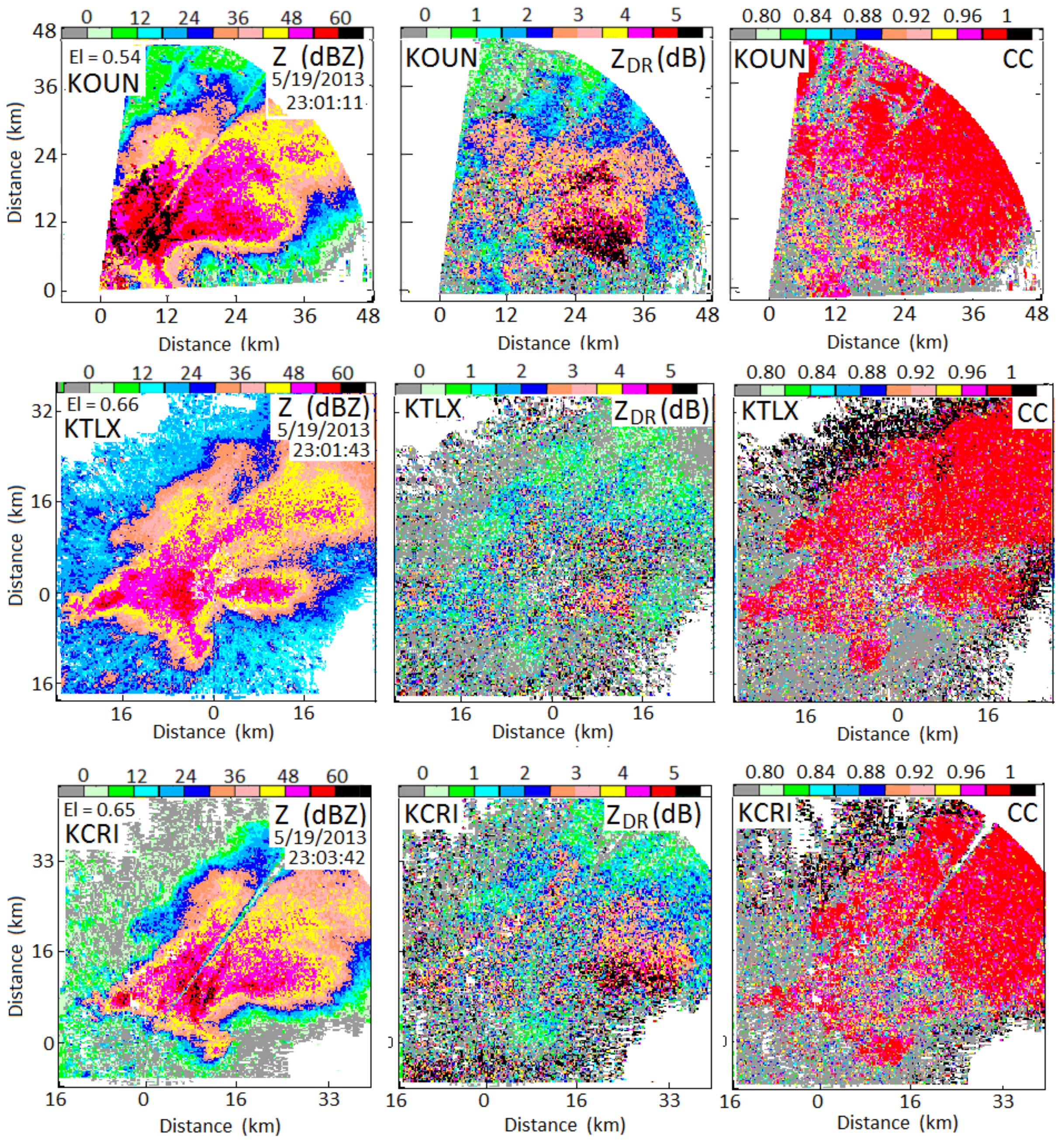

Fig. 7. Polarimetric fields collected with KOUN, KTLX, and KCRI on May 19, 2013 at about 23:01 UTC.

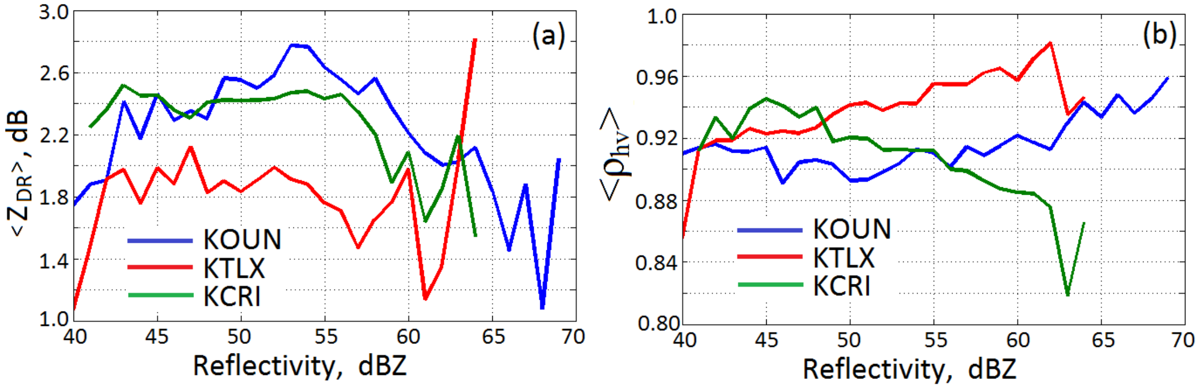

Fig. 8. (a): The mean Z_{DR} as a function of reflectivity for event 19 May, 2013. (b): Same as in (a) but for the mean correlation coefficients.

In Fig. 8, the mean <Z_{DR}> and <ρ_{hv}> as functions of Z are shown. Again, maximal reflectivity from KOUN is 5 dB larger than those from KTLX and KCRI and the difference in <Z_{DR}> from KOUN and KTLX is about 1 dB for Z < 60 dBZ. Values of <ρ_{hv}> are noticeably lower than those for the previous event.

The following conclusion can be drawn from data collected from the two tornadic cases.

- Maximal reflectivity values from KOUN are frequently larger than those from other two WSR-88Ds, i.e., KTLX and KCRI. It should be noted that KOUN operates at lower frequency than KTLX and KCRI.

- ZDR values from KOUN are larger than those from KTLX by about 1 dB, which is a substantial number that cannot be attributed to miscalibration of differential reflectivities in the systems.

- The correlation coefficients did not show noticeable drops in areas with giant hail. There seems to be no indications on drops in <ρ_{hv}> with increasing Z. Dependences of <ρ_{hv}> on radar frequencies have not been revealed.

3. Impacts of radar parameters on hail recognition

The WSR-88D radars operate at S frequency band 2700 – 3000 MHz. Adjacent WSR-88Ds operate at slightly different frequencies to reduce interference signals. Hailstones are not small compared to the radar wavelength therefore radar characteristics of hail exhibit resonant features even inside the S band. Experiments conducted on two WSR-88Ds with different frequencies show different reflectivity values in hail cores (Melnikov et al. 2010). So one of radar parameters that impact measured reflectivity and differential reflectivity is radar frequency. Another radar parameter is differential phase in transmit ψ_t; we show its impacts on the differential phase upon scattering and correspondingly on the correlation coefficient.

3.1. Impacts of radar frequency

Carrier frequencies of adjacent WSR-88D radars are offset to reduce signal interference. Changes in carrier frequencies slightly change radar parameters such as the antenna beamwidth, waveguide losses, and receiver sensitivity. An automatic calibration procedure, running on all radars, brings reflectivity values to the same level with accuracy of 1 dB. The radar calibration procedure is based on basic engineering principles and assumes same scattering properties of weather echoes. One of the missions of the WSR-88Ds is precipitation measurement. The maximal stable size of raindrops is 6 mm which is small compared to the wavelength, i.e., 10 cm, so that the Rayleigh approximation for scattering properties are often used for rain. Sizes of hailstones can be a few centimeters and the Rayleigh approximation cannot be used in calculation of their scattering properties. For spherical hailstones, Mie theory is used. It follows from the theory that the radar cross section is an oscillating function of the diameter and wavelength so that radar backscattering cross sections and corresponding reflectivities are different at different wavelengths. This is frequently called the resonant effect highlighting strong oscillations of scattering cross sections as functions of size or wavelength. This effect is used for hail detection with a two-wavelength radar, 3- and 10-cm, i.e., at X- and S-bands (Atlas and Ludlum 1961, Eccles and Atlas 1971, Doviak and Zrnic 2006, section 8.5.1) and at C- and S-bands (Féral et al. 2003), i.e., at highly diverse frequencies.

For radars operating in a narrow frequency band, it is assumed that small deviations of carrier frequencies do not change radar cross section substantially so that reflectivities are the same within the band. Melnikov et al. (2010) analyzed this assumption for rain and hail for the WSR-88D's frequency band and showed that the resonant effect can cause a noticeable difference in reflectivity measured with adjacent WSR-88Ds. This means that adjacent radars, that use slightly different carrier frequencies, will measure different reflectivity values due to the resonant effect if hail is present.

The difference of measured reflectivity values at wavelengths λ_1 and λ_2 is

$$Z_{\lambda 1} - Z_{\lambda 2} = 10 \log[\int \sigma(D, \lambda_1) N(D) dD / \int \sigma(D, \lambda_1) N(D) dD], \quad (dB) \qquad (1)$$

where $N(D)$ is the size distribution, i.e., the number of particles with diameter D in the unit volume and $\sigma(D,\lambda)$ is the backscatter cross section of the scatterer. This difference depends on the wavelengths and sizes of hydrometeors. To calculate radar reflectivity for hailstones, we utilized the T-matrix method (Mischenko et al. 2002).

If hail is present in the radar volume, the difference of radar cross sections can reach several dB. Dry hailstones do not contain water on their surface or within. If there is a water film on the surface of a hailstone, such hailstones are usually called wet. Spongy hailstones consist of a mixture of ice and water.

Size distributions $N(D)$ of hailstones can be quite diverse. Smaller sizes have been represented by an exponential function or a gamma function (Cheng and English 1983, Federer and Wladvogel 1975) but large sizes often seem to have narrow distributions centered on the mean (Ziegler et al. 1983). Thus we consider different $N(D)$. Results for a uniform distribution between *Dmin* and *Dmax* with *Dmax* - *Dmin* = 1 cm are presented in Fig. 9(a) as a function of *Dmax*. It is seen that the reflectivity difference can exceed 2 dB for hailstones with diameters larger than 3.5 cm and reaches 6 dB at *Dmax* = 4.5 cm for wet hailstones. For exponential distributions, shown in Figs. 9(b), the Z difference can be 2 dB for *Dmax* in the interval 3.5 to 5 cm. In our calculations, we used Λ=0.3 (Doviak and Zrnic 2006, section 8.1.3) in $N(D) = N\text{o} \exp(-\Lambda D)$.

Two general conclusions can be deduced from Fig. 9. 1) Resonant effects can produce a reflectivity difference at close wavelengths as high as 6 dB and higher than 2 dB in a large interval of hailstones diameters from 3.5 to 5 cm. 2) The reflectivity difference can be positive and negative; it is mainly positive for hailstones with diameters smaller than 4.5 cm and it is mainly negative for larger diameters. From these conclusions we deduce that if the hailstone diameter is smaller than 4.5 cm, KOUN reflectivity values can exceed reflectivity values from KCRI. For larger hailstones, the opposite can happen, i.e., KCRI's reflectivity values can be larger than KOUN's reflectivity values. This could explain the first observed feature that was stated in the end of section 2.

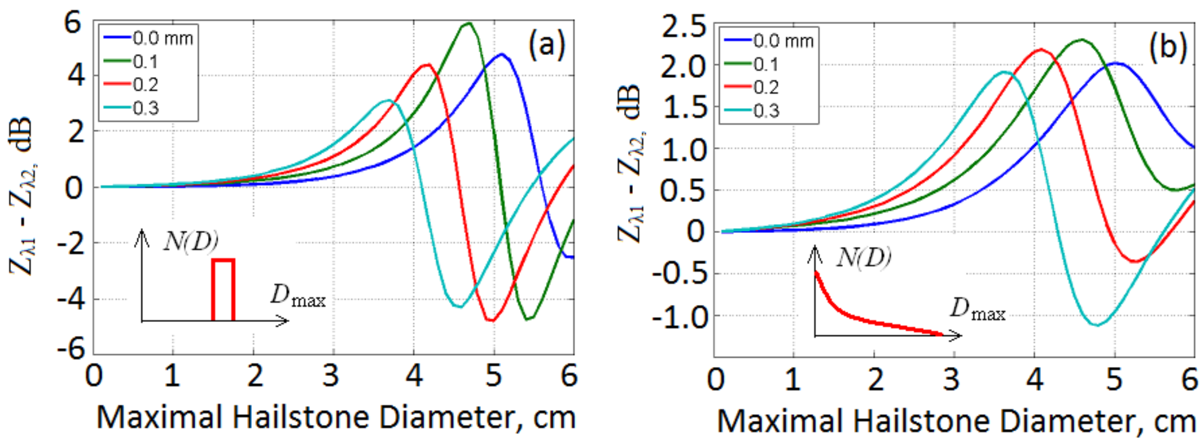

Fig. 9. (a): The difference of reflectivity values of hailstones at two wavelengths corresponding to KOUN (λ=11.1 cm) and KCRI (λ=10.0 cm for two forms of size distributions shown in the inserts. The thickness of water films on hailstones is indicated in the legends.

Radar observations show that hail can have positive and negative Z_{DR}. Usually positive Z_{DR}, is associated with oblate hailstones falling with the major axis being about horizontal. Negative Z_{DR} is usually associated with conical hailstones falling with the major axis being vertical. Resonant effects make this consideration more complicated: nonspherical scatterers experience different resonances at different dimensions. In Fig. 10(a), one can see that oblate scatterers produce negative Z_{DR} for diameters larger than about 50 mm. A similar feature exhibits prolate hailstones (Fig. 10c). This is in contrast to rain wherein oblate raindrops produce positive Z_{DR} only. The difference of Z_{DR}, measured at two wavelengths remains close to zero for prolate and oblate hailstones with sizes less than 5 cm. Thus differences in Z_{DR} measured from two WSR-88Ds point to the presence of very large hailstones with diameters larger than 5 cm. This could explain the second observed issue stated in the end of section 2 if we assume prolate hailstones as it is shown in Fig. 5.

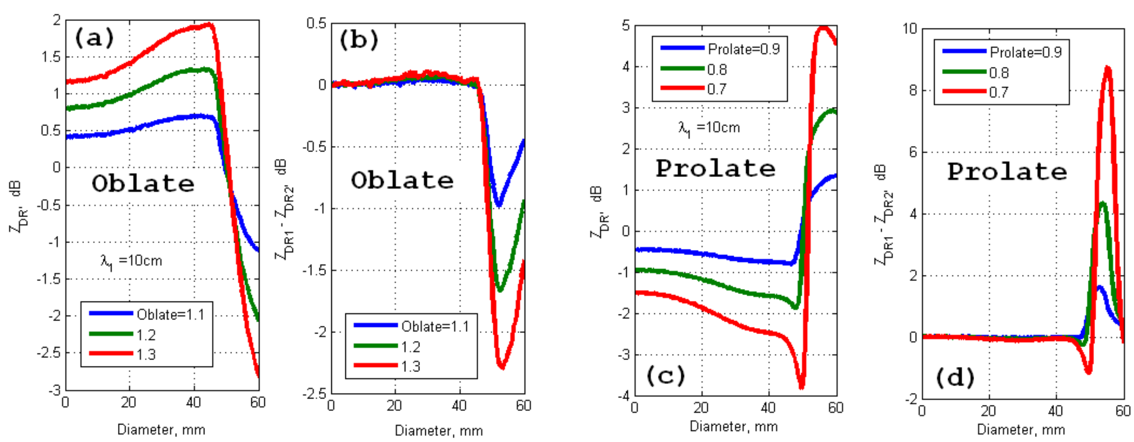

Fig. 10. (a): Differential reflectivity of oblate ice spheroids with oblateness 1.1, 1.2, and 1.3 and (b) the difference of Z_{DR} at two wavelengths corresponding to KOUN (λ=11.1 cm) and KCRI (λ=10.0 cm). (c) and (d) same as in (a) and (b) but for prolate spheroids.

3.2. Impacts of differential phase in transmit

The dual-polarization WSR-88D radars employ a configuration with Simultaneously Transmitted And Received (STAR) horizontally and vertically polarized waves (Doviak et al. 2000). In the STAR radars, signal paths in the two radar channels with horizontally and vertically polarized waves are different so the transmitted and received waves acquire hardware phase shifts in transmit, ψ_t, and in receive, ψ_r. A medium with nonspherical scatterers shifts the phase between the horizontally and vertically polarized waves by the propagation differential phase Φ_{DP} and differential phase upon scattering δ so that the measured phase shift is $\psi_{dp} = \psi_t + \psi_r + \Phi_{DP} + \delta$. It can be shown that the phase in receive ψ_r does not affect differential reflectivity and correlation coefficient. In contrast to this, phase ψ_t affects Z_{DR} and $\rho_{hv.}$

Large hailstones frequently have nospherical shape that means they do not tumble randomly in the air. To acquire nonspherical shapes, hailstones should precess in the air, most likely. Such preceesing can lead to positive Z_{DR} which are observed in hail cores frequently. Precessing affects the differential phase upon scattering and correlation coefficient. The differential phases upon scattering as functions of the azimuthal angle (viewing angle) are shown in Fig. 11a for different ψ_t. The hailstone was modeled with a wet prolate spheroid with the maximal size of 4 cm and axis ratio (width/length= *b/a*) of 0.8. It is seen that ψ_t affects δ significantly. Fig. 11b presents dependences of and ρ_{hv} upon ψ_t for different *b/a*. The hailstones are assumed to precess around the vertical axis with the mean canting angle of 30°. Zero canting angle corresponds to rotation of the prolate spheroid on the horizontal plane. One can see that the incident differential phase affects ρ_{hv} significantly.

The incident differential phase is the sum $\psi_t + \Phi_{DP}$. Since this phase depends upon Φ_{DP} its impact on measured differential phase and ρ_{hv} can be different for the same hail core observed from different directions having different Φ_{DP}. Fig. 11b can be used to explain the third issue observed in the events (section 2) and stated in the end of section 2: the incident phases for the three WSR-88Ds used to collect the data can be different due to different ψ_t, which can lead to different measured correlation coefficients.

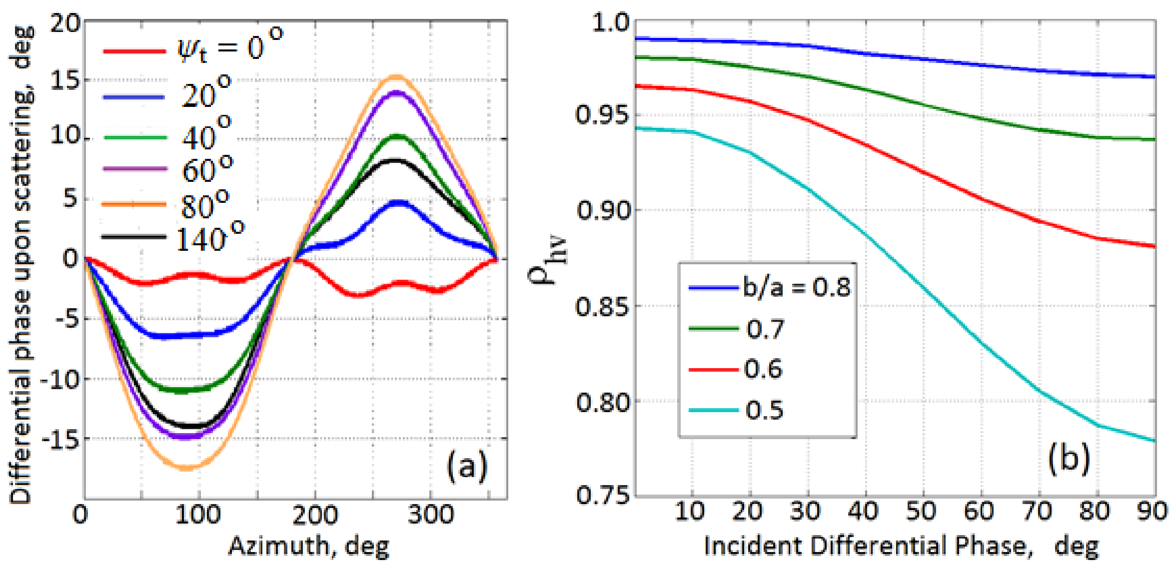

Fig. 11. (a): Differential phase upon scattering by a prolate wet hailstone precessing/rotating over azimuth as a function of azimuth and the incident differential phase ψ_t. The maximal size of the hailstone is 3 cm, the axis ratio is 0.8, and the mean canting angle of precession is 60°. (b): The correlation coefficient for rotating prolate wet hailstones as in (a) as a function of ψ_t and the axis ratio b/a.

4. Some other observed features of tornadic hailstorms

Low ZDR and ρ_{hv} are the most prominent features of the tornado debris balls (Ryzhkov et al. 2003a). In the following subsection, we discuss applicability of another polarimetric parameter to identify tornado debris. In subsection 4.2, we show fields of a new dual polarization parameter, which can be used to locate inflow regions into severe thunderstorms.

4.1. SDR values

STAR radars are capable of measuring STAR Differential Ratio (SDR) introduced by Melnikov and Matrosov (2013). SDR is a proxy of Circular Depolarization Ratio (CDR) that can be measured with radar with circular polarization in transmit and receive. CDR is a measure of deviations of scatterers' shape from a sphere. For nearly spherical scatterers, CDR measured in dB is of order of -30 dB, which is close to a limit achievable in weather radars. The CDR values increase with increasing axis ratios of scatterers, which is the ratio of major to minor axes. CDR cannot be measured with the WSR-88D but SDR exhibits properties similar to ones of CDR.

SDR is determined from differential reflectivity in power units (Zdr) and the correlation coefficient as,

$$SDR = \frac{Z_{dr} + 1 - 2Z_{dr}^{1/2}\rho_{hv}}{Z_{dr} + 1 + 2Z_{dr}^{1/2}\rho_{hv}}.$$

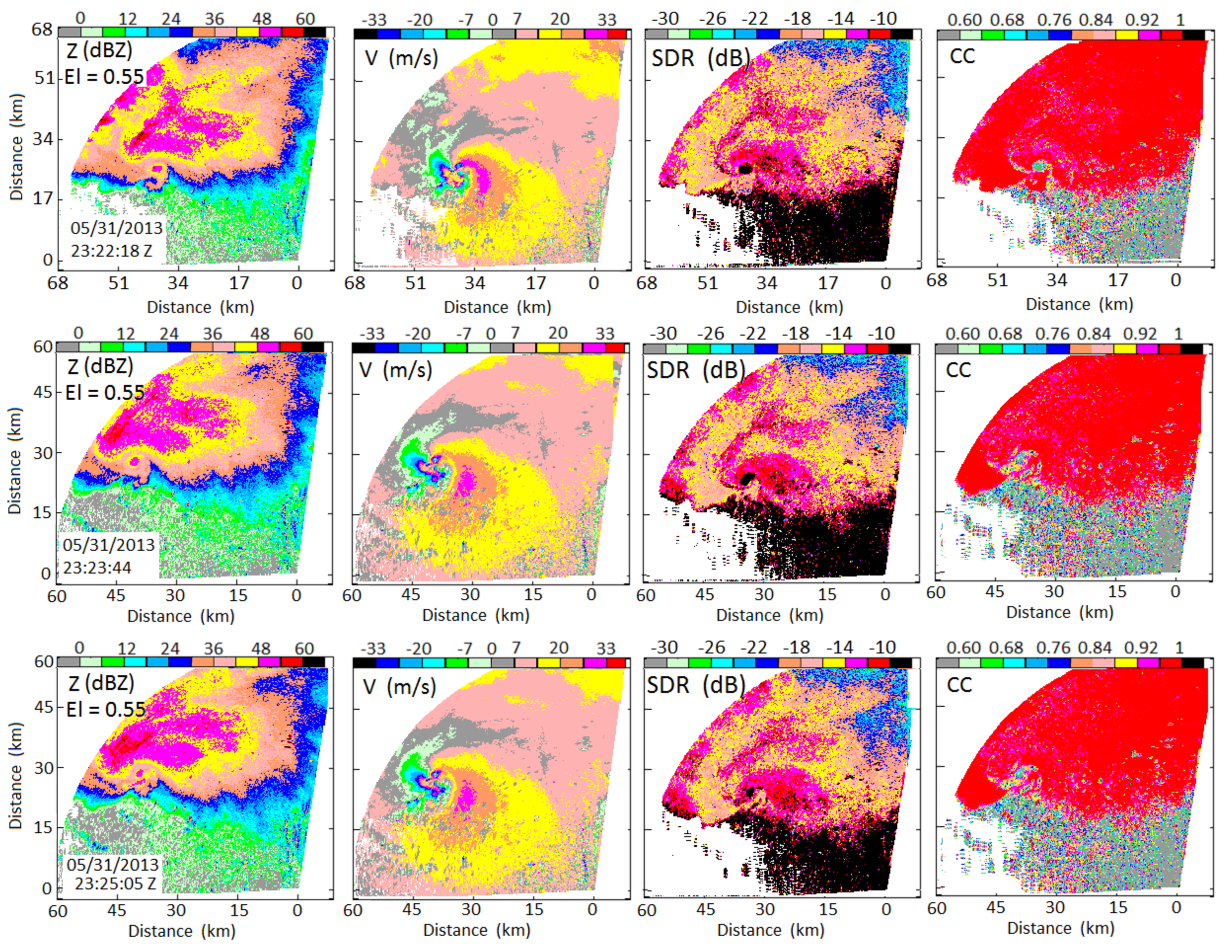

Fig. 12. (top row): Fields of reflectivity, the Doppler velocity, SDR, and correlation coefficient collected with WSR-88D KOUN at the lowest antenna elevation on May 31, 2013 at 23:22:18 UTC. (Central and bottom rows): same as in the top raw but at 23:23:44 and 23:25:05 UTC.

An interval of SDR values for the WSR-88Ds is from -30 to -10 dB for clouds and precipitation and can reach 0 dB in echoes from insects and birds. The 20-dB interval of SDR values for hydrometeors is much wider than the typical interval of ZDR values from 0 to 5 dB.

Fig. 12 presents the polarimetric fields of a tornadic thunderstorm observed 31 May, 2013. All fields exhibit tornado features, i.e., a hook echo (Z), a mesocyclone (V), and low ρ_{hv} values in the tornado debris ball. It is seen in the SDR fields that this parameter has values larger than -10 dB in the tornado area. SDR values there are similar to those in the echoes from insects in the low right corner of the panels. This means that tornado area is filled with highly nonspherical scatterers. A close look reveals differences in the SDR and ρ_{hv} fields that can be used to further characterize scatterers in tornado zones.

4.2. The differential Doppler velocity as a precursor of the wind inflow areas

Six radar variables are measured with polarimetric Doppler weather radars; these are equivalent reflectivity factor, the Doppler velocity, spectrum width, Z_{DR}, Φ_{DP}, and ρ_{hv}. Reflectivity and the Doppler velocity (V_h) are measured at horizontal polarization. The Doppler velocity can be obtained at vertical polarization (Vv) as well and the differential Doppler velocity (DDV) can be obtained as, DDV = $V_h - V_v$. In weather echoes, the absolute values of DDV are less than 0.5 m s^{-1}. DDV can exceed 5 m s^{-1} in echoes from insects and birds. Fields of reflectivity, Doppler velocity, and DDV in echoes from two tornadic thunderstorms are presented in Figs. 13. Hook echoes at the southern edge of each supercell thunderstorm (Fig. 13) are clearly seen. It is known that strong inflows frequently take place in hook echoes. The DDV field in the hook areas exhibit very large values of both signs (Fig. 13c) and the areas are likely filled with insects and birds. The large DDV values in the hook areas are not due to reduced signal-to-noise ratios. DDV values in the northern edges of the storms with similar reflectivity exhibit DDV of weather values. It is remarkable that the radar captures such a feature at distance of 100 km where tornado velocity signatures are not exhibited due to a wide area covered with the radar beam.

It is also seen from Fig. 13c that the absolute DDV values in the thunderstorm are less than 0.5 m s^{-1}. Two more features should be noted in the DDV field. 1) At distances closer than 40 km from the radar, the DDV field is granular. These DDV are caused by insects and birds. 2) There is a well pronounced area with very large negative DDV around coordinates 120 km to the west and 25 km to the north from the radar. Relative to the radar location, this area lays behind a strong reflectivity cell at 100km West and 20km South. The area behind the zone with large negative DDV has a "finger"-like echo stretching from the core out to a range of 150 km. This echo is the result of "three body scattering" frequently observed in strong hail cores. A part of radar radiation gets scattered by the core to the ground which reflects it back to the core and the core scatters it back to radar (e.g., Zrnic et al. 2010). Different intensities of scattered and reflected radiation at horizontal and vertical polarizations produce large DDV. This is not DDV from cloud particles only; reflection from the ground plays a critical role. A complete analysis of this feature is out of the scope of this study.

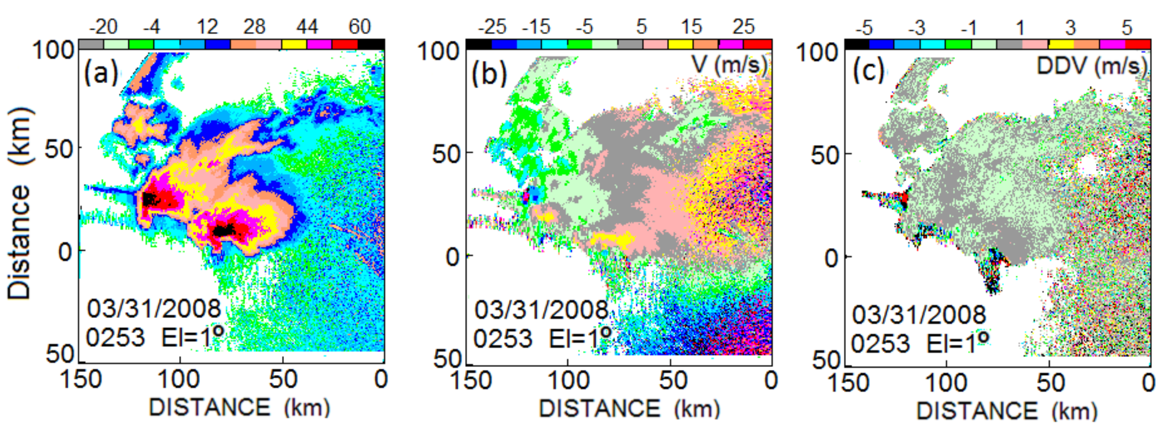

Fig. 13. Fields of reflectivity, the Doppler velocity, and DDV collected with WSR-88D KOUN on March 31, 2008 at 0253 UTC.

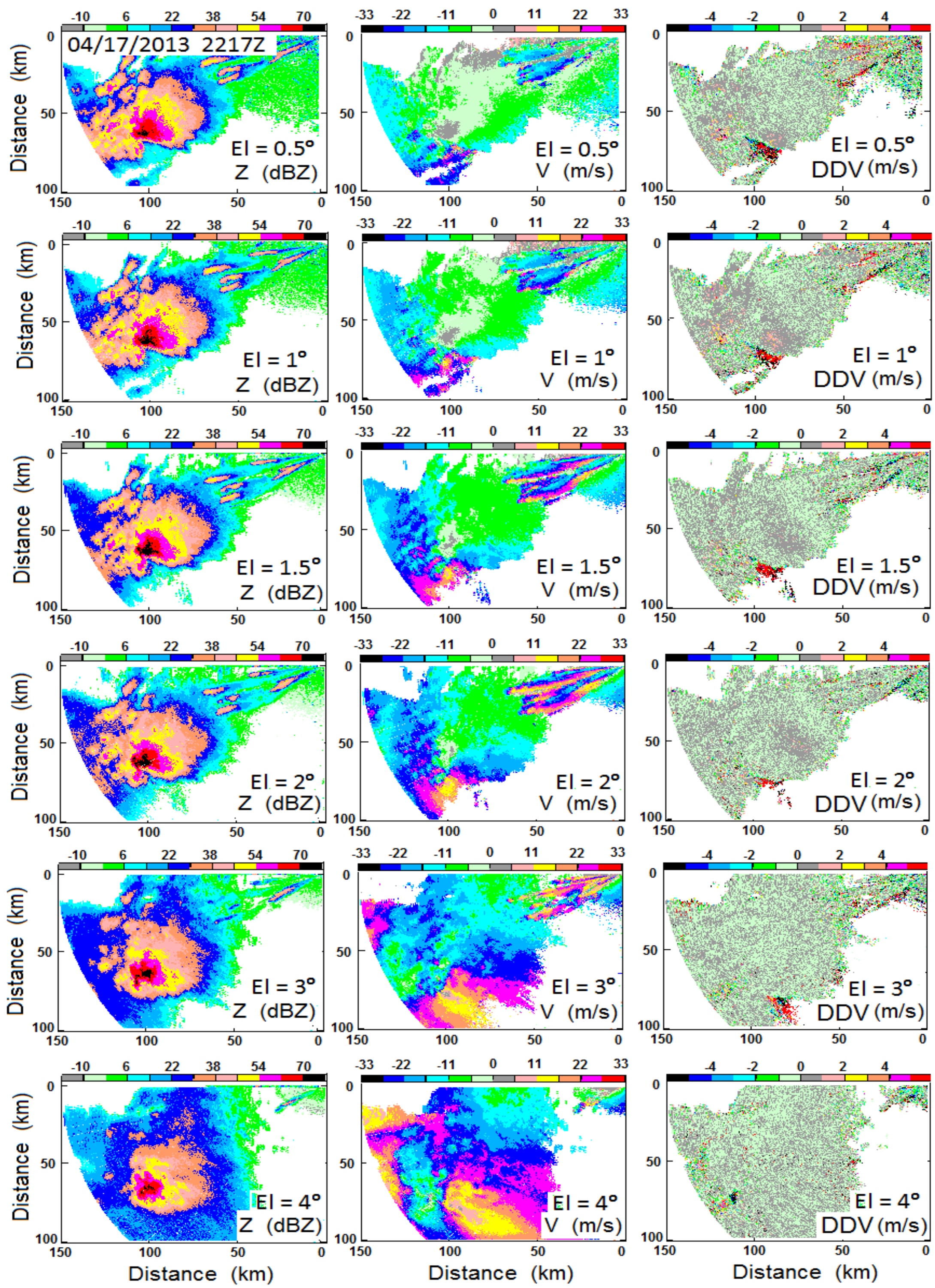

Fig. 14. (top row): Fields of reflectivity, the Doppler velocity, and DDV collected with WSR-88D KOUN on April 17, 2013 at 2217 UTC at antenna elevation of 0.5°. (following rows): same as in the top row but at different antenna elevations.

One more case is shown in Fig. 14. The data were collected in a hailstorm with significant mesocyclone rotation seen at elevations from 1 to 3^{o} in the area of hook echo (but a tornado was not spawned). Areas with large DDV values are clearly seen in the field of typical “weather“ DDV values. These areas are seen up to 3^{o} elevation, i.e., at heights of 4 km from the ground. So it can be concluded that the inflow area stretched up to 4 km height.

5. Conclusions

Our observations of tornadic hailstorms showed severe attenuation of X band radiation; in the events in May 2013 it was so severe that radiation did not reach the hail cores (Figs. 2,4). Therefore data in the hail cores were available only from three S band radars, i.e., KOUN, KTLX, and KCRI.

We have analyzed data collected with three S band radars in the same areas of high reflectivities in the thunderstorms and observed differences in radar variables (section 2.2): reflectivity values, Z_{DR} and ρ_{hv} are different for radars operating at different frequencies. Our calculations show that the difference in frequency about 200 MHz can change reflectivity and Z_{DR} by a few dB in areas containing hail (section 3.1). This effect is a manifestation of resonant nature of scattering by hailstones.

The system differential phase in transmit can alter measured ρ_{hv} for radars with the STAR polarimetric configuration implemented in the WSR-88Ds (section 3.2). This effect is a consequence of depolarization of signals scattered by nonspherical hailstones. Therefore measured correlation coefficients can be different for two radars operating at the same frequency but having different system differential phase in transmit.

Dual-polarization parameter SDR can be used to estimate the axis ratio (length/width) of scatterers (section 4.1). SDR values in the tornado balls can be very large (Fig. 12) compared to typical values in precipitation.

Dual-polarization parameter DDV (Differential Doppler Velocity, i.e., the difference of Doppler velocities measured at horizontally and vertically polarizations) is not larger than 0.5 m s^{-1} in clouds and precipitation and can reach 5-7 m s^{-1} in echoes from insects and birds (section 4.2). In tornadic and hail thunderstorms, we noticed that areas of inflow exhibit large DDV values (Fig. 14) that could be due to ingested/trapped insects in inflow areas. The inflow area in Fig. 14 stretched up to height of 4 km.

References

Atlas, D., and F. H. Ludlum, 1961: Multi-wavelength radar reflectivity of hailstorms. *Quart. J. Roy. Meteor. Soc.*, **87,** 523–534.

Balakrishnan, N., and D.S. Zrnic, 1990: Use of polarization to characterize precipitation and discriminate large hail. *J. Atmos. Sci.*, **47,** 1525-1540.

Bringi, V.N., V. Chandrasekar, N. Balakrishnan, and D.S. Zrnic, 1990: An examination of propagation effects on radar measurements at microwave frequencies. *J. Atmos. Oceanic Technol.*, **7,** 829-840.

Burgess, D.W., V. Melnikov, D. Priegnitz, R. A. Brown, P. Heinsleman, E. Mansel, and V. Wood , 2014: Tornadic supercells in central Oklahoma on May 19, 20, and 31 of 2013: NSSL radar data. *94-th AMS annual meeting. Special Symposium on Severe Local Storms.* Atlanta, GA, AMS.

Cheng, L., and M. English, 1983: A relation- ship between hailstone concentration and size. *J. Atmos. Sci.* **40,** 204-213.

Doviak, R. J. and D. S. Zrnic, 2006: *Doppler radar and weather observations*, 2nded., Dover Publications, 562 pp.

Eccles, P. J., and D. Atlas, 1973: A dual-wavelength radar hail detector. *J. Appl. Meteor.*,**12,** 847–854.

Federer, B., and Wladvogel, 1975: Hail and raindrop size distributions form a Swiss multicell storm. *J. Appl. Meteor.*, **14,** 91-97.

Féral, L., H. Sauvageot, and S. Soula, 2003: Hail detection using S and C-band radar reflectivity difference. *J. Atmos.Oceanic Technol.*, **20,** 233–248.
Heinselman, P.L., and A.V. Ryzhkov, 2006: Validation of polarimetric hail detection. *Weather and Forecasting*, **21,** 839-850.

Kumjian, M.R., and A.V. Ryzhkov, 2008: Polarimetric signatures in supercell thunderstorms. *J. Appl. Meteor. Climat.*, **48,** 1940-1961.

Kumjian, M.R., and A.V. Ryzhkov, 2009: Storm relative helicity revealed from polarimetric radar measurements. *J. Atmos. Sci.*, **66,** 667-685.

Melnikov, V., R. Lee, and N. Langlieb, 2010: Hail reflectivity signatures from two adjacent WSR-88Ds: carrier frequency and calibration issues. *26th Conference on Interactive Information and Processing Systems (IIPS) for Meteorology, Oceanography, and Hydrology***.** Phoenix, AZ, AMS**.** Available online at https://ams.confex.com/ams/90annual/webprogram/Paper161721.html

Melnikov, V. and S. Matrosov, 2013: Radar measurements of the axis ratios of cloud particles, 36th Weather Radar Conf., Breckenridge, CO, AMS.

Melnikov, V., M. Leskinen, and J. Koistinen, 2014: Doppler velocities at orthogonal polarizations in radar echoes from insects and birds, *IEEE Geosci. Remote Sens. Letters*, DOI: 10.1109/LGRS.2013.2272011.

Miller, L.J., J.D. Tuttle, and C.A. Knight, 1988: Airflow and hail growth in a severe Northern High Plains supercell. *J. Atmos. Sci.*, **45,** 736-762.

Mischenko M. I., L.D. Travis, and A.A. Lacis, 2002: *Scattering, Absorbtion, and Emission of Light by Small Particles.* Cambridge University Press, 228 pp.

Picca, J., A. Ryzhkov, 2012: A dual-wavelength polarimetric analysis of the 16 May 2010 Oklahoma City extreme hailstorm. *Mon. Wea. Rev.*,**140**, 1385–1403.

Ryzhkov, A.V., T. J. Schuur, D. W. Burgess, and D. S. Zrnic, 2005a: Polarimetric tornado detection. *J. Appl. Meteor.*, **44,** 557-570.

Ryzhkov, A.V., T.J. Schuur, D.W. Burgess, P. L. Heinselman, S. E. Giangrande, and D. S. Zrnic, 2005b: The joint polarization experiment. *Bull. Amer. Meteor. Soc.*, **86,** 809-824.

Schwarz, C.M. and D.W. Burgess, 2011: Supercell polarimetric signatures at X-Band: Data from VORTEX2. Extended Abstracts, *35th Conf. Radar Meteorology*, Pittsburgh, Pennsylvania, United States, Amer. Meteor. Soc., 7B.4., [Available online at http://ams.confex.com/ams/35Radar/webprogram/Paper191298.html]

Witt, A., M. D. Eilts, G. J. Stumpf, J. T. Johnson, E. De W. Mitchell, K. W. Thomas, 1998: An Enhanced Hail Detection Algorithm for the WSR-88D. *Wea. Forecasting*, **13**, 286–303.

Ziegler C.L., P.S. Ray, and N. C. Knight, 1983: Hail growth in an Oklahoma mutlicell storm. *J. Atmos. Sci.* **40,** 1768-1791.

Zrnic, D.S., G. Zhang, V. Melnikov, J. Andric. "Three-body scattering and hail size". *J. Appl. Meteor. Climatol.* Vol. 49, N 4, pp. 687–700, April 2010.